Electronic Supplementary Material (ESI) for Journal of Materials Chemistry A.

Supporting Information

Interfacial engineering in amorphous/ crystalline heterogeneous nanostructures as a highly effective battery-type electrode for hybrid supercapacitors

Dongyan Gao[a], Yifan Pan[a], Jinhe Wei[a], Dandan Han[a,*], Pengcheng Xu[a], Yen Wei[b,*], Liucheng Mao[b], Xiaohong Yin[c]

[a] *College of Chemistry and Pharmaceutical Engineering, Jilin Institute of Chemical Technology, Jilin 132022, China*
[b] *Department of Chemistry and the Tsinghua Center for Frontier Polymer Research, Tsinghua University, Beijing, 100084, China*
[c] *School of Chemistry and Chemical Engineering, Tianjin University of Technology, Tianjin 300384, China*

*Corresponding author.
E-mail address: handandan@jlict.edu.cn (D.H.); weiyen@tsinghua.edu.cn (Y.W.)

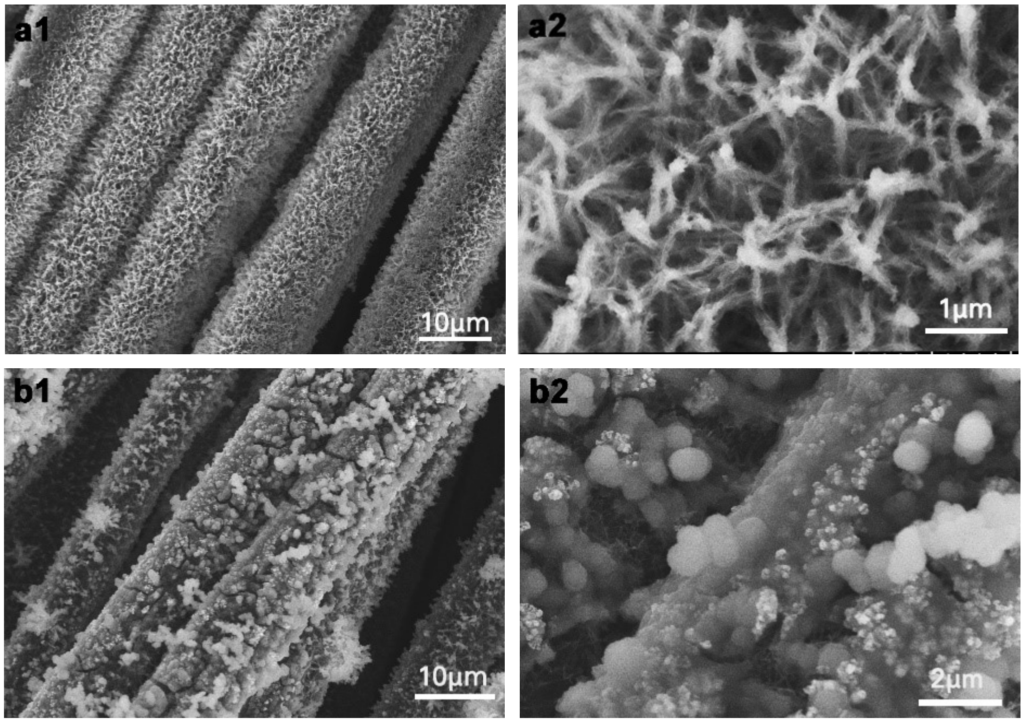

Figure S1. (a1, a2) SEM images of CC/$NiCo_2O_4$@NiCo-P-2 and (b1, b2) SEM images of CC/$NiCo_2O_4$@NiCo-P-8.

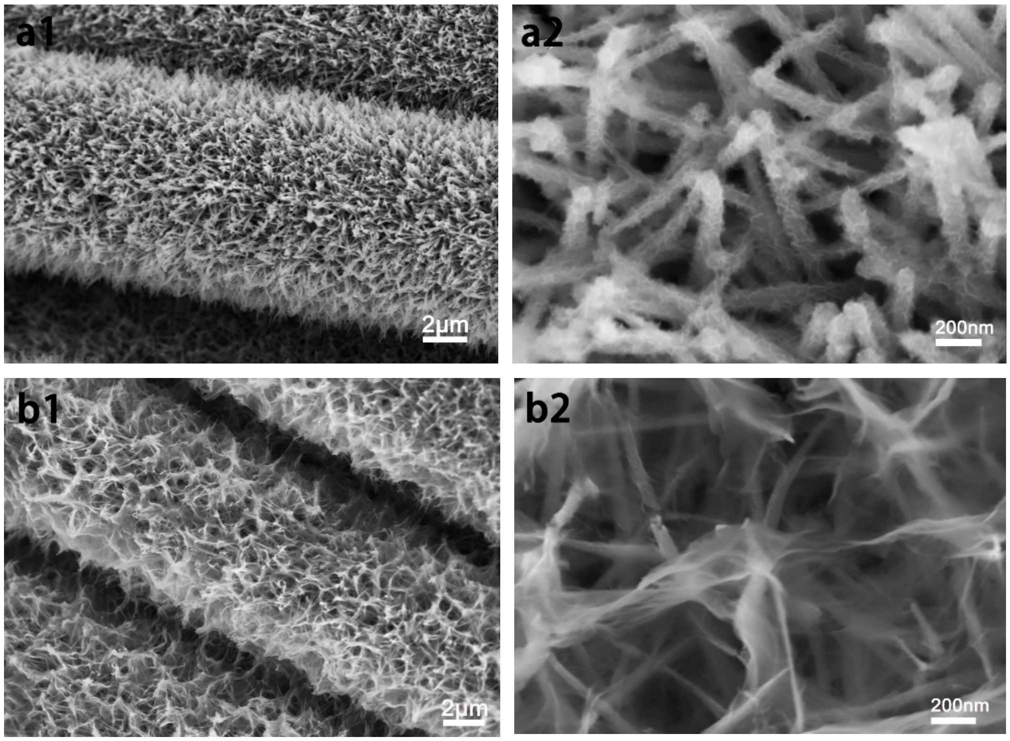

Figure S2. (a1, a2) SEM images of CC/$NiCo_2O_4$@Ni-P-5 and (b1, b2) SEM images of CC/$NiCo_2O_4$@Co-P-5.

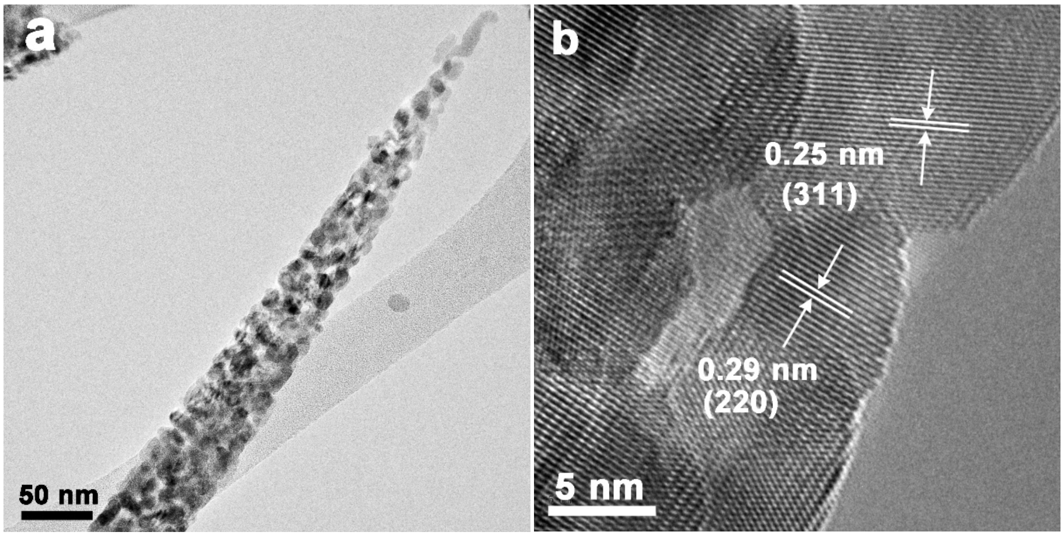

Figure S3. TEM images of $NiCo_2O_4$ nanowires.

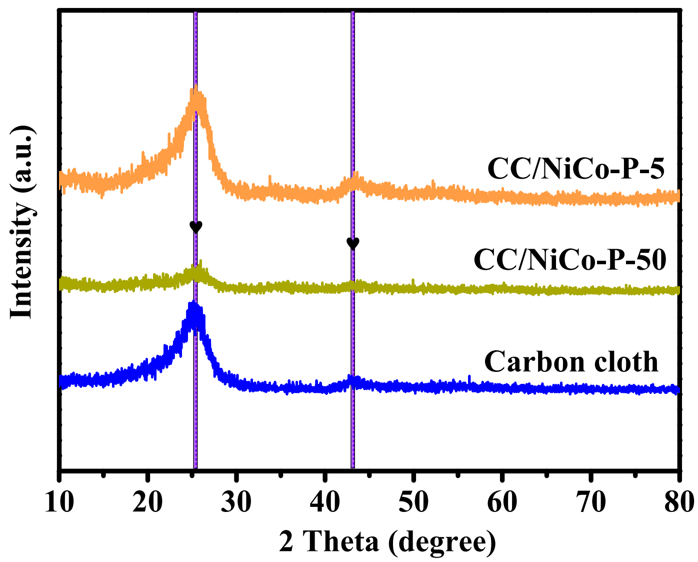

Figure S4. XRD patterns of amorphous CC/NiCo-P-5 nanosheets with different deposition time. Obviously, when the deposition time is 5 cycles, there is no diffraction peaks except for the diffraction peaks of carbon cloth. In order to eliminate the influence of the weak signal caused by the amount of the sample, the deposition time was extended to 50 cycles. It can be noted that some weak diffraction peaks are corresponding to carbon cloth, which is attributed to the reason that the amorphous phosphate encapsulates the carbon cloth (the diffraction peak intensity is reduced by this thickened package).

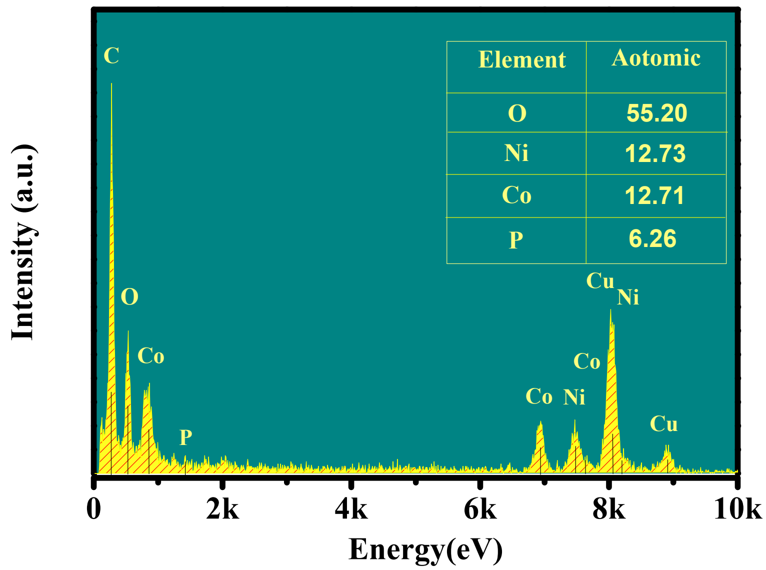

Figure S5. EDX spectrum of CC/$NiCo_2O_4$@NiCo-P-5

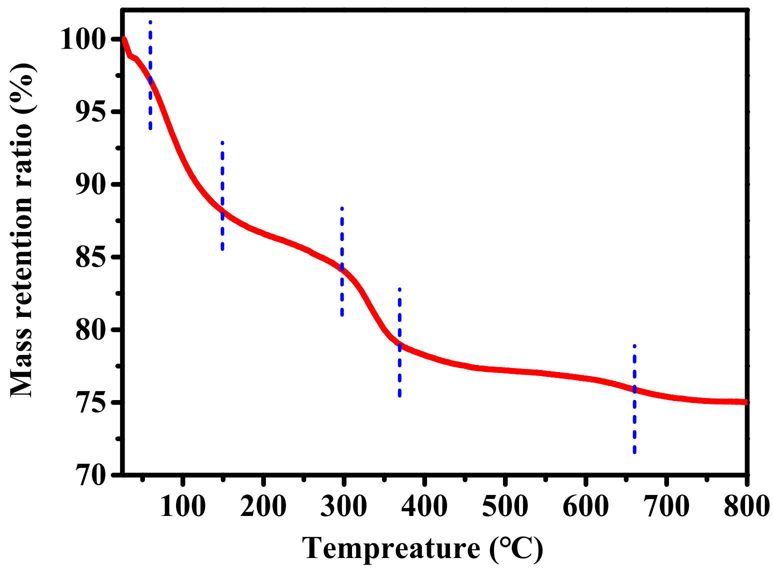

Figure S6. TGA analysis curve of the CC/NiCo-P-5 with a rising rate of 10℃·min^{-1} from 25 to 800 ℃ at N_2 atmosphere. A weight loss was about 12% from 25 to 150 ℃, owing to the decomposition of physically absorbed water and some residual alcohol on the surface of the sample. A weight loss was about 5.5% from 300 to 370 ℃, which attributed to the decomposition of structural water. After 400 ℃, the mass remained basically unchanged. Therefore, TGA data, coincident with the results mentioned above (EDX, XPS and so on), further indicate that the molecular formula of amorphous substance can be calculated as NiCo-$(HPO_4)_2 \cdot H_2O$.

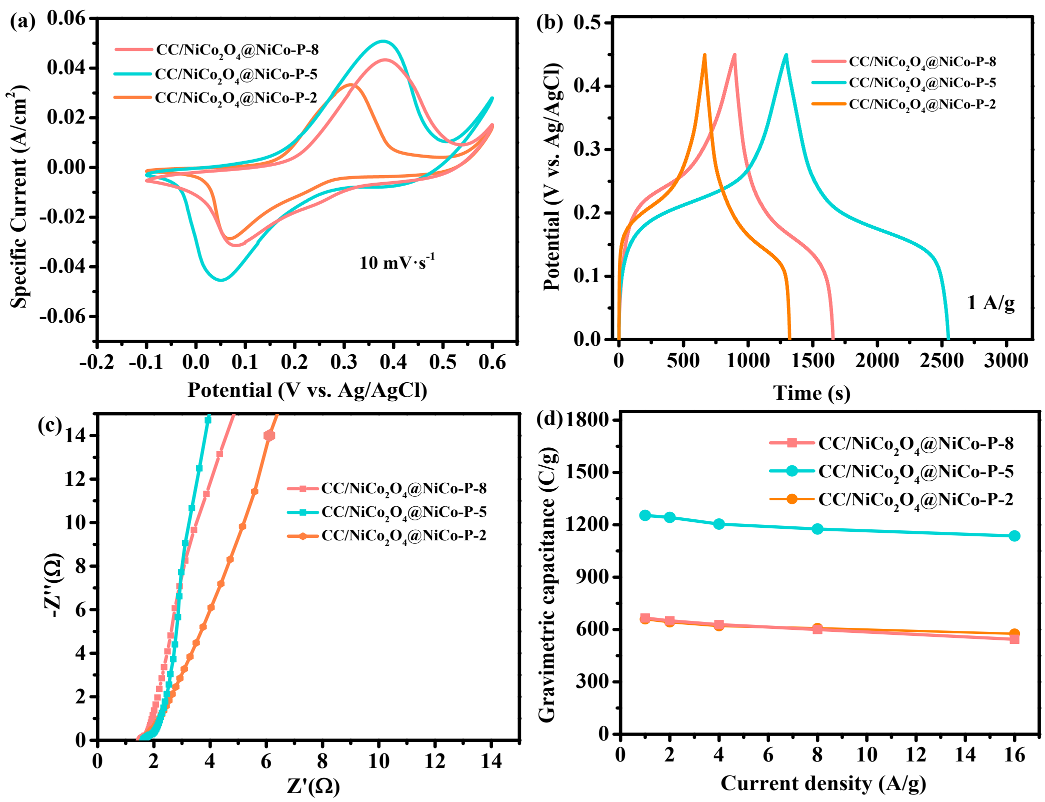

Figure S7. Comparison of electrochemical performance between CC/$NiCo_2O_4$@NiCo-P-8, CC/$NiCo_2O_4$@NiCo-P-5 and CC/$NiCo_2O_4$@NiCo-P-2 electrodes: (a) CV curves at 10 $mV \cdot s^{-1}$. (b) GCD curves at 1$A \cdot g^{-1}$; (c) Nyquist plot of the three electrodes; (d) Specific capacity at different specific currents.

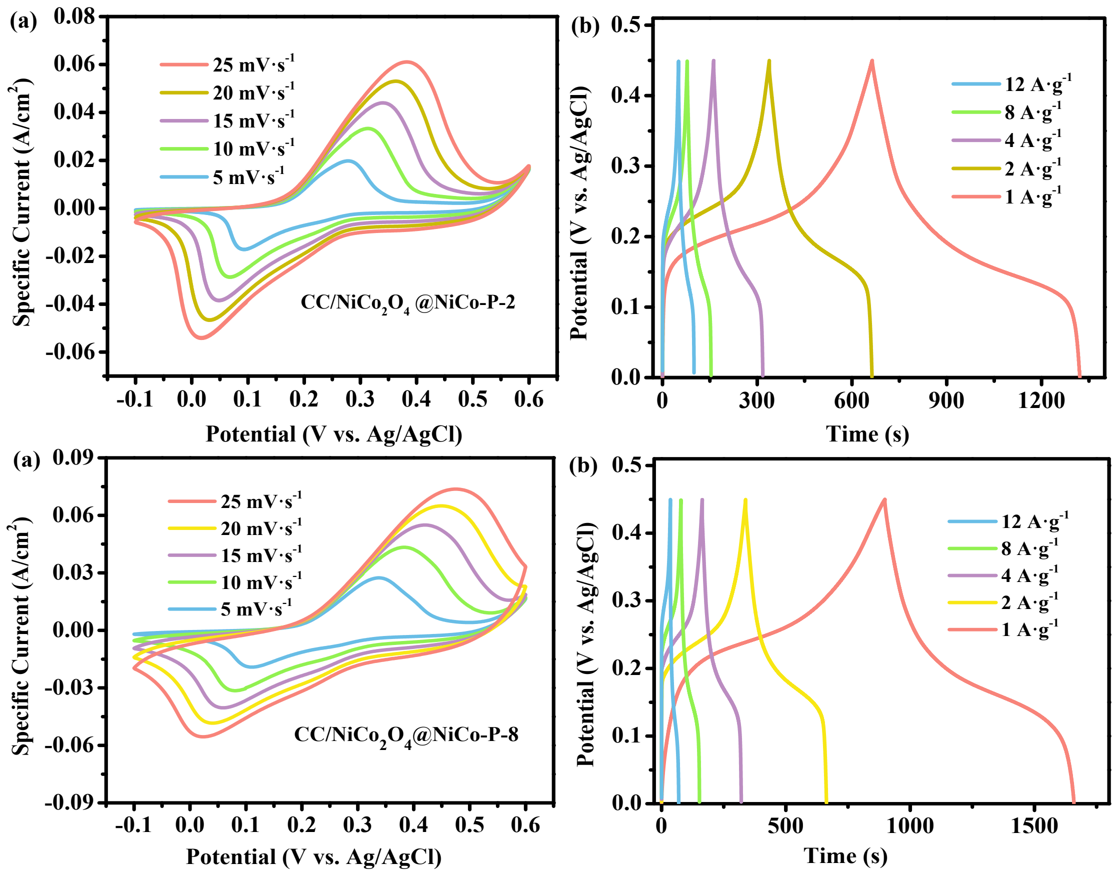

Figure S8. (a) CV curves and (b) GCD curves of CC/$NiCo_2O_4$@NiCo-P-2. (a) CV curves and (b) GCD curves of CC/$NiCo_2O_4$@NiCo-P-8.

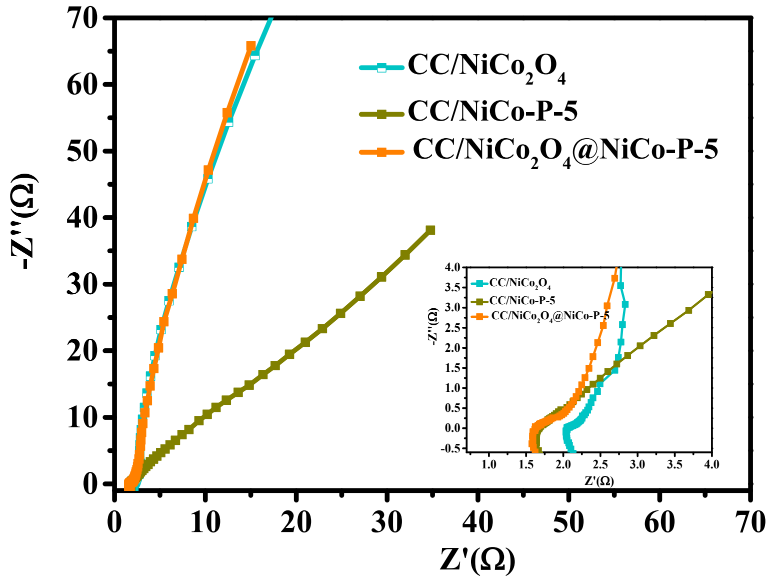

Figure S9. Nyquist plot of CC/$NiCo_2O_4$@NiCo-P-5, CC/NiCo-P-5 and CC/$NiCo_2O_4$.

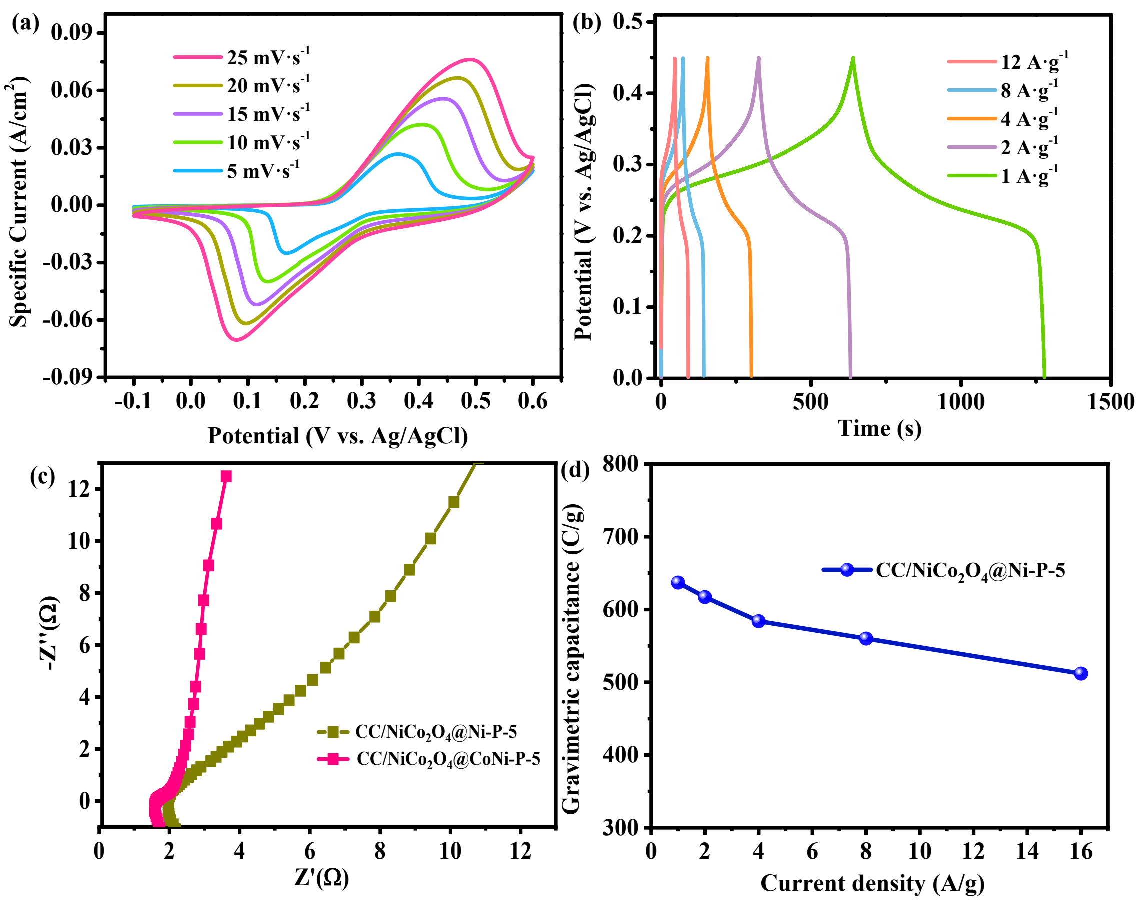

Figure S10. (a) CV curves and (b) GCD curves of CC/$NiCo_2O_4$@Ni-P-5. (c) Nyquist plot in the frequency of 10 kHz to 0.01 Hz. (d) specific capacities of CC/$NiCo_2O_4$@Ni-P-5.

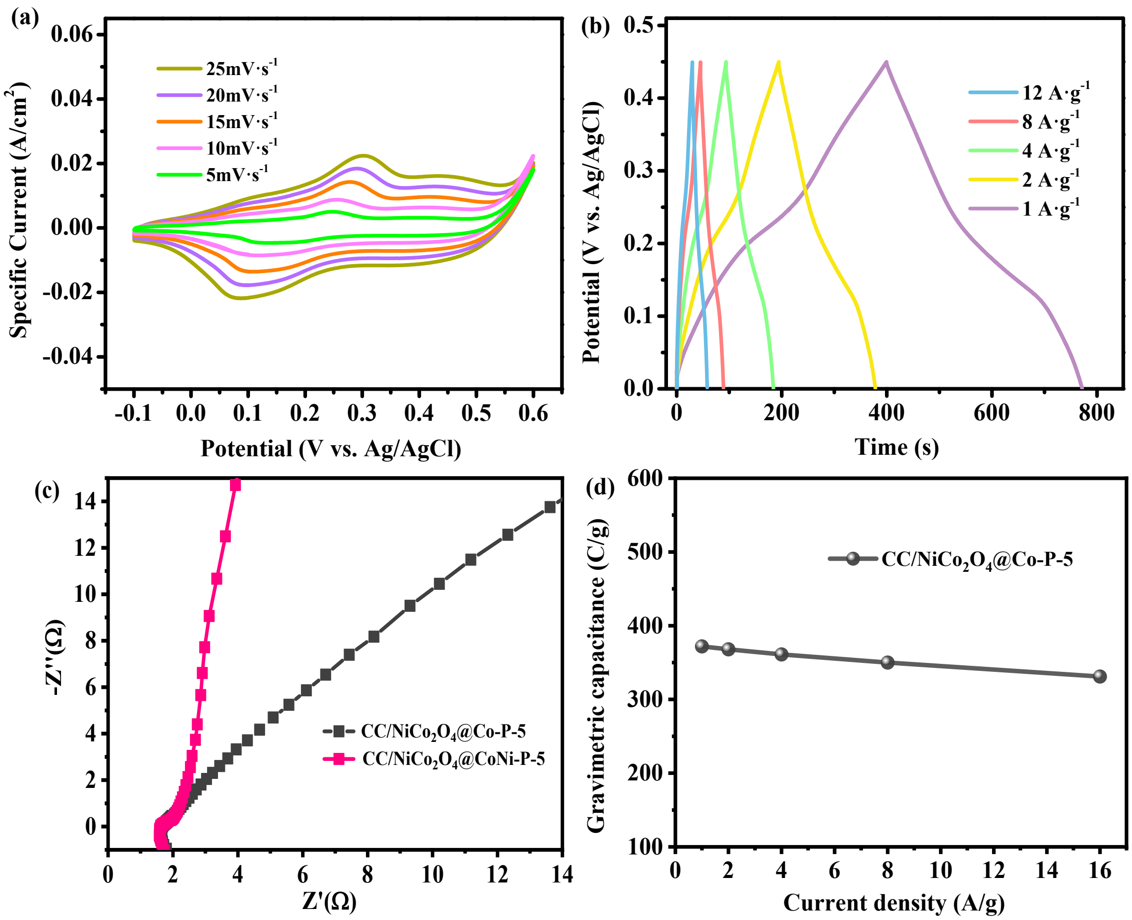

Figure S11. (a) CV curves and (b) GCD curves of CC/$NiCo_2O_4$@Co-P-5. (c) Nyquist plot in the frequency of 10 kHz to 0.01 Hz. (d) specific capacities of CC/$NiCo_2O_4$@Co-P-5.

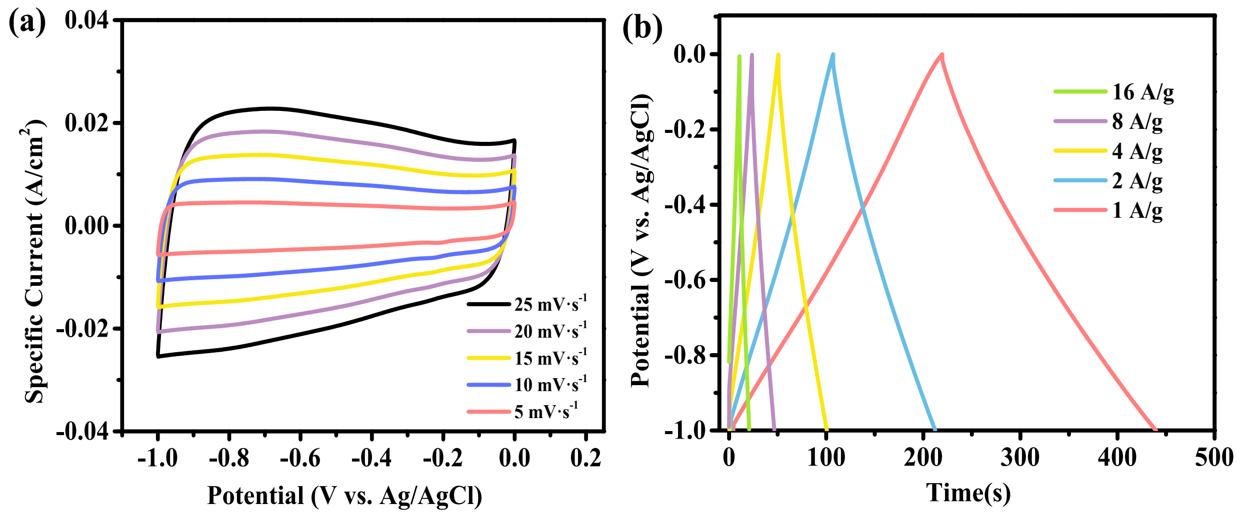

Figure S12. (a) CV curves and (b) GCD curves of AC HSC device.

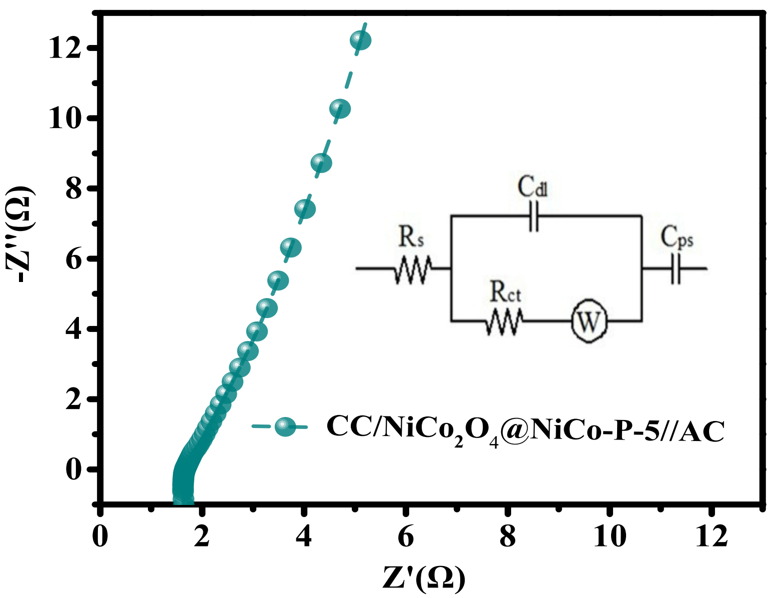

Figure S13. Nyquist plots of the CC/$NiCo_2O_4$@NiCo-P-5//AC HSC device; the insets show the high-frequency range and equivalent circuit used to simulate the Nyquist plots.

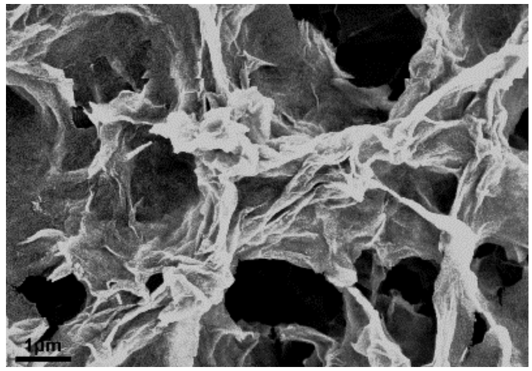

Figure S14. SEM images of CC/$NiCo_2O_4$@NiCo-P-5 after cycling

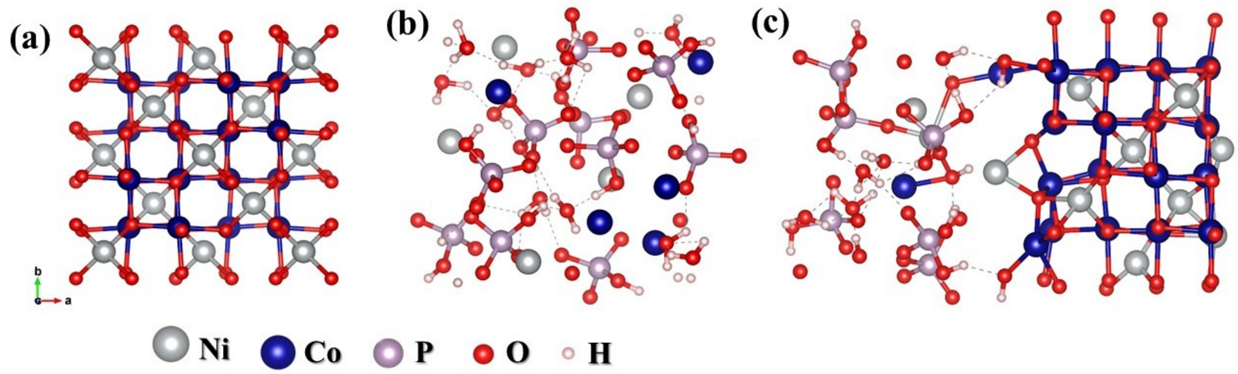

Figure S15. Optimized atomic structure models of (a) $NiCo_2O_4$, (b) NiCo-P and (c) $NiCo_2O_4$@NiCo-P

Table S1. Comparison of electrochemical performances of the amorphous electrode material with previous reports.

Materials	Electrolyte	Capacity	Reference
amorphous cobalt hydrogen phosphate	2M KOH	176.82 C/g (1 A/g)	J. Power Sources 449 (2020) 227487
amorphous Ni-Co double hydroxide	2M KOH	768.15 C/g (1 A/g)	Nanoscale 13 (2021) 8562-8574
amorphous Co-Ni pyrophosphates	3M KOH	692.45 C/g (1.5 A/g)	ACS Appl. Mater. Interfaces 8 (2016) 23114-23121
amorphous Mn_3O_4	1M NaOH	298 C/g (1 mA/cm^2)	ACS Appl. Mater. Interfaces 11 (2019) 39394
Amorphous Vanadium Oxides	5 M LiCl	346 C/g (0.625 A/g)	Chem. Eng. J. 403 (2021) 126380
amorphous Ni-Co-Fe hydroxide	4M KOH	805 C/g (6.4 A/g)	Adv. Energy Mater. 5 (2015) 1401767
amorphous Co_3O_4	1M KOH	226.1 C/g (1.3 A/g)	Chem. Eng. J. 396 (2020) 125364
amorphous nickel borate	6M KOH	496.44 C/g (0.2 mV/s)	J. Mater. Chem. A. 6 (2018) 19689-19695
amorphous $NiCo(HPO_4)_2 \cdot H_2O$	**2M KOH**	**688 C/g (1 A/g)**	**This work**

Table S2. Comparison of electrochemical performances of the amorphous/crystalline heterostructure electrode material with previous reports.

Materials	Electrolyte	Capacity	Reference
amorphous MoS_x@crystalline $FeCo_2O_4$	3M KOH	978 C/g (1 A/g)	Chem. Eng. J. 417 (2021) 127927
crystalline Ag@amorphous nickel-cobalt hydroxide	6M KOH	718.1 C/g (1 A/g)	Adv. Mater. Interfaces 6 (2019) 1900858
crystalline $Ni_2P_2O_7$@amorphous NiCo-OH	2M KOH	35.36 C/g (3 mA/cm^2)	Small 10 (2019) 1901145
crystalline Ni_3S_4@amorphous MoS_2	6M KOH	576.36 C/g (2 A/g)	Small 11 (2015) 3694-3702
crystalline/amorphous $Fe_2O_{3-\delta}$	1 M LiOH	630.9 C/g (6 A/g)	Nano Energy 45 (2018) 390-397
crystalline/amorphous Co_3S_4	2M KOH	815.4 C/g (5 mA/cm^2)	J. Mater. Chem. A. 6 (2018) 21350-21359
crystalline ZIF-67@amorphous ZIF	6M KOH	470.7 C/g (1 A/g)	J. Mater. Sci. 55 (2020) 16360-16373
amorphous Ni-Co-S@crystalline MnS	PVA/KOH	1093 C/g (1 A/g)	Chem. Eng. J. 416 (2021) 129500
$NiCo_2O_4$@$NiCo(HPO_4)_2\cdot H_2O$	**2M KOH**	**1254 C/g (1 A/g)**	**This work**